

Characterization of Two Mitochondrial Flavin Adenine Dinucleotide-Dependent Glycerol-3-Phosphate Dehydrogenases in *Trypanosoma brucei*

Ingrid Skodová, Zdenek Verner, Frédéric Bringaud, Peter Fabian, Julius Lukes and Anton Horváth
Eukaryotic Cell 2013, 12(12):1664. DOI:
10.1128/EC.00152-13.
Published Ahead of Print 18 October 2013.

Updated information and services can be found at:
<http://ec.asm.org/content/12/12/1664>

SUPPLEMENTAL MATERIAL	<i>These include:</i> Supplemental material
REFERENCES	This article cites 47 articles, 14 of which can be accessed free at: http://ec.asm.org/content/12/12/1664#ref-list-1
CONTENT ALERTS	Receive: RSS Feeds, eTOCs, free email alerts (when new articles cite this article), more»

Information about commercial reprint orders: <http://journals.asm.org/site/misc/reprints.xhtml>
To subscribe to to another ASM Journal go to: <http://journals.asm.org/site/subscriptions/>

Characterization of Two Mitochondrial Flavin Adenine Dinucleotide-Dependent Glycerol-3-Phosphate Dehydrogenases in *Trypanosoma brucei*

Ingrid Škodová,^{a,b} Zdeněk Verner,^{a,b,d} Frédéric Bringaud,^c Peter Fabian,^{a*} Julius Lukeš,^{b,d} Anton Horváth^a

Department of Biochemistry, Comenius University, Bratislava, Slovakia^a; Biology Centre, Institute of Parasitology, Czech Academy of Sciences, České Budějovice (Budweis), Czech Republic^b; Centre de Résonance Magnétique des Systèmes Biologiques, UMR 5536, Université Bordeaux Segalen, Bordeaux, France^c; Faculty of Sciences, University of South Bohemia, České Budějovice (Budweis), Czech Republic^d

Glycerol-3-phosphate dehydrogenases (G3PDHs) constitute a shuttle that serves for regeneration of NAD⁺ reduced during glycolysis. This NAD-dependent enzyme is employed in glycolysis and produces glycerol-3-phosphate from dihydroxyacetone phosphate, while its flavin adenine dinucleotide (FAD)-dependent homologue catalyzes a reverse reaction coupled to the respiratory chain. *Trypanosoma brucei* possesses two FAD-dependent G3PDHs. While one of them (mitochondrial G3PDH [mtG3PDH]) has been attributed to the mitochondrion and seems to be directly involved in G3PDH shuttle reactions, the function of the other enzyme (putative G3PDH [putG3PDH]) remains unknown. In this work, we used RNA interference and protein overexpression and tagging to shed light on the relative contributions of both FAD-G3PDHs to overall cellular metabolism. Our results indicate that mtG3PDH is essential for the bloodstream stage of *T. brucei*, while in the procyclic stage the enzyme is dispensable. Expressed putG3PDH-V5 was localized to the mitochondrion, and the data obtained by digitonin permeabilization, Western blot analysis, and immunofluorescence indicate that putG3PDH is located within the mitochondrion.

Trypanosoma brucei is a unicellular parasite causing African sleeping sickness in humans and nagana in cattle. It is widespread in sub-Saharan regions, rendering vast areas unusable for herding. Drugs used for the treatment of trypanosomiasis in humans are highly toxic and difficult to administer (1). Hence, new drug targets are urgently needed.

The main proliferative stages of *T. brucei* are the long-slender bloodstream form (BF) in mammals and the procyclic form (PF) residing in the midgut of the tsetse fly vector *Glossina* spp. The two forms differ significantly in their energy and metabolic transduction pathways. The PF consumes mainly amino acids proline and threonine, which are abundantly present in the tsetse fly (2). This stage has a fully developed mitochondrion containing a full complement of cytochromes and most of the enzymes of the Krebs cycle (2, 3). Unexpectedly, however, the Krebs cycle does not work as a true cycle such as is seen in other eukaryotes, since it uses various intermediates produced by the amino acid metabolism as sources of reducing equivalents (4), which are then oxidized via a classical respiratory chain (2).

As a consequence of their glucose-rich environment, the BF cells totally depend on glycolysis for ATP production, as the ATP-generating functions of its mitochondrion are repressed (5). The respiratory chain of the BF consists only of a trypanosomal alternative terminal oxidase (TAO) and a flavin adenine dinucleotide (FAD)-dependent glycerol-3-phosphate dehydrogenase (FAD-G3PDH) (6). Whereas, together with the other Krebs cycle enzymes, respiratory complex II is missing in the BF (5), complex I is present, although its contribution to the electron flow remains uncertain (7, 8).

Glycolysis, confined in kinetoplastid flagellates to a specialized organelle termed the glycosome (9), is connected with mitochondrial respiration via the glycerol-3-phosphate:dihydroxyacetone phosphate shuttle (G3P:DHAP). This shuttle consists of two enzymes: FAD-G3PDH, located on an outer face of the inner

mitochondrial membrane (10), and NAD-dependent glycerol-3-phosphate dehydrogenase (NAD-G3PDH), located in the glycosomes (6). The main distinction of this pathway in Kinetoplastida compared to other eukaryotes is the noncytosolic localization of NAD-G3PDH (11). Sequestration of the first seven steps in the glycosome (5) makes glycolysis independent of the cytosolic NADH/NAD⁺ ratio. The essential glycolytic NAD⁺ production is covered either by the succinate-producing glycosomal pathway in PF (9, 12) or by the G3P:DHAP shuttle in BF. In BF, electrons from G3P are shuffled by FAD-G3PDH to ubiquinol in the mitochondrial respiratory chain, resulting in the production of ubiquinone, which is oxidized by the TAO, the only terminal oxidase transferring electrons to oxygen (13). In PF, the FAD-G3PDH is expressed, although its involvement in metabolism is not essential (14).

Trypanosomal NAD-G3PDH is encoded by a single gene, in contrast to yeast and plants, which carry more isoforms with different functions in their genomes (15, 16). On the other hand, *T. brucei* and *Leishmania major* surprisingly code for two FAD-G3PDH genes, a situation not described in any other organism. In

Received 3 July 2013 Accepted 14 October 2013

Published ahead of print 18 October 2013

Address correspondence to Julius Lukeš, jula@paru.cas.cz, or Anton Horváth, horvath@fns.uniba.sk.

* Present address: Peter Fabian, Institute of Molecular Genetics, Czech Academy of Sciences, Prague, Czech Republic.

I.Š. and Z.V. contributed equally to this article.

Supplemental material for this article may be found at <http://dx.doi.org/10.1128/EC.00152-13>.

Copyright © 2013, American Society for Microbiology. All Rights Reserved.
doi:10.1128/EC.00152-13

the genome of *T. brucei*, they are annotated as mitochondrial FAD-G3PDH (Tb11.02.5280; mtG3PDH) and putative FAD-G3PDH (Tb927.1.1130; putG3PDH). The subcellular localization of the latter dehydrogenase is unknown, being *in silico* predicted by MitoCarta (<http://www.broadinstitute.org/pubs/MitoCarta/index.html>) to have mitochondrial localization (17), or its putative N-terminal signal peptide can possibly target this protein to the endoplasmic reticulum (see www.genedb.org entry for Tb927.1.1130). Mitochondrial localization of mtG3PDH was experimentally confirmed by ectopic expression in yeast (14), and this result was subsequently confirmed by a high-throughput tandem affinity purification (TAP)-tag-based proteomic analysis (18) (compare results for mt- and putG3PDH at www.trypsinproteome.org). Later, involvement of mtG3PDH in the procyclic glycosome redox balance was described as an alternative pattern of glycosomal succinate production (12). However, a functional analysis of trypanosomal G3PDH enzymes and their overall role(s) in mitochondrial and cell metabolism has been lacking.

Therefore, the aim of this study was to determine the subcellular localization and physiological importance of both G3PDH enzymes in the model flagellate *T. brucei*.

MATERIALS AND METHODS

Organisms used and growth conditions. The procyclic form (PF) of *T. brucei* (strain 29-13) was cultivated as described previously (27) at 27°C in SDM-79 medium containing 10% (vol/vol) heat-inactivated fetal bovine serum, 7.5 µg/ml hemin, 50 µg/ml hygromycin, and 15 µg/ml G418, with 2.5 µg/ml phleomycin being added as a selection agent for a transgenic RNA interference (RNAi) strain. Transgenic cells expressing V5-tagged putative G3PDH (putG3PDH-V5) have been selected by the addition of 15 µg/ml puromycin. Bloodstream form (BF) *T. brucei* (strain 427; single marker) was cultured as described previously (6) at 37°C with 5% CO₂ in HMI-9 medium supplemented with 28 mg/liter bathocuproinedisulfonic acid, 182 mg/liter L-cysteine, 121 mg/liter hypoxanthine, 0.0014% (vol/vol) 2-mercaptoethanol, 110 mg/liter pyruvate, 39 mg/liter thymidine, 10% (vol/vol) heat-inactivated fetal bovine serum, 3.1 µg/ml hygromycin, and 2.5 µg/ml phleomycin.

For localization studies, *Saccharomyces cerevisiae* strain L5366 (ura3) was grown on LB either in culture or on agar plates. Selection of strain putG3PDH-yEGFP (representing a fusion with yeast-enhanced green fluorescent protein [yEGFP]) was carried out using minimal medium agar plates containing yeast nitrogen base (YNB) supplemented with 0.4 mg/liter adenine, 0.4 mg/liter histidine, 0.4 mg/liter tryptophan, 0.6 mg/liter lysine, 0.6 mg/liter leucine, and 2% (wt/vol) glucose; 0.4 mg/liter methionine was added to suppress the expression of the pUG35 plasmid. For localization assays, methionine was omitted and glucose or 3% (wt/vol) glycerol was used as a carbon source.

T. brucei cells were counted using a Z2 Coulter Counter. Cell cultures were diluted 10 times as soon as they reached concentrations of 10⁷ and 10⁶ cells/ml for PF and BF, respectively. The *S. cerevisiae* cell concentration was established using the optical density at 600 nm (OD₆₀₀), assuming that OD₆₀₀ = 1 is equal to 8 × 10⁶ cells/ml. For expression assays, cells in the logarithmic phase were used.

Construction of cell lines and RNAi. The *T. brucei* PF and BF were transfected with the RNAi p2T7-177 vector (19), allowing ablation of the mitochondrial FAD-G3PDH. This construct was prepared by cloning a PCR-amplified fragment of the region spanning nucleotides 493 to 1303 of the FAD-G3PDH gene (Tb11.02.5280). An 810-bp-long amplicon generated using a forward primer (5'-CGGATCCAACAAGTGGTGAAGGC AACC-3') (BamHI restriction site underlined) and a reverse primer (5'-AAGCTTCCCACAACACTCACCATCAG-3') (HindIII site underlined) was cloned into the pCR2.1-TOPO TA vector (Invitrogen), cut out using

the added restriction sites, and recloned into the p2T7-177 vector. Finally, the resulting construct was linearized using NotI and 10 µg of DNA was electroporated into the PF and BF cells. For selection of transformants, phleomycin was added 24 h after electroporation, and clones were obtained as described elsewhere (20). Synthesis of double-stranded RNA (dsRNA) was induced by the addition of 1 µg/ml tetracycline (tet) to the medium.

The whole open reading frame (ORF) of the putG3PDH gene (Tb927.1.1130) was amplified by PCR using a forward primer (5'-AAAG CTTATGGGTCGCTATACGCG-3') (added HindIII site underlined) and a reverse primer (5'-TGGATCCACACTCTCGGCACC-3') (BamHI site underlined) and cloned into pCRII-TOPO (Invitrogen). Upon verification by sequencing, the ORF was cut out via the added restriction sites and cloned into the predigested pLew79 plasmid (21) bearing a V5 tag (22). A 10-µg volume of the resulting vector was NotI linearized prior to electroporation into PF *T. brucei* cells. Transformants were selected with puromycin (15 µg/ml) added 1 day after electroporation, and the expression was induced by 1 µg/ml tet as described above.

For heterologous expression in *Saccharomyces cerevisiae*, putG3PDH was amplified using a forward primer (5'-GTCTAGACAATGGGTCGCT ATACGC-3') (XbaI site underlined) and a reverse primer (5'-CATAAA GCTTGTGAGAGCCGTGGC-3') (added HindIII site underlined), and the PCR product was cloned into pCR4-TOPO (Invitrogen). Upon sequencing, the ORF was cut out using added restriction sites and cloned into pUG35 (23). Transformation of yeast was carried out following standard protocols (24).

RNAi was evaluated using real-time quantitative PCR (qPCR). To this end, total RNA was extracted using TRIzol reagent (Invitrogen) according to the manufacturer's protocol, and 15 µg of RNA was treated with 4 U of DNase and the appropriate buffer in a total volume of 50 µl at 37°C for 30 min (Turbo DNase kit; Ambion). Following the incubation, an additional 2 U of DNase was added and the reaction was stopped after 30 min by the addition of 10 µl of DNase inhibitor. RNA was coprecipitated with 5 µg glycogen (Invitrogen) in a mixture of ice-cold 96% ethanol and 50 mM sodium acetate. To prepare templates for qPCR, cDNA was synthesized from 5 µg RNA using SuperScript III reverse transcriptase (RT; Invitrogen) and random hexamers, with a parallel reaction mixture lacking the enzyme used as a negative control. Both cDNA reaction mixtures were diluted 1:10 in water prior to qPCR, which was performed using a Rotor-Gene 3000 real-time DNA detection system thermocycler. Data were acquired using Rotor-Gene v.6.1 software (Corbett Life Science). A housekeeping 18S rRNA transcript served as a reference (25). For the detection of mtG3PDH transcripts, a forward primer (5'-TGTCTCGTATTCCTG AGAAG-3') and a reverse primer (5'-GGCGTTTCTGGTAGAGAAG-3') (4 µl each from 1.5 µM stock) were added to a 20-µl reaction mixture containing 10 µl of Power SYBR green PCR Master Mix (Applied Biosystems) and 2 µl of the cDNA. In the case of the reference gene, the cDNA was additionally diluted 1:50 in water. The samples were subjected to the following qPCR program: 2 min at 50°C, 10 min at 95°C, and 40 cycles of 15 s at 95°C and 60 s at 60°C. Fluorescence was detected at the end of the latter step. The relative abundance levels of RNAs of induced and noninduced samples were determined by the Pfaffl method (26).

Spliced leader RNA. cDNA, prepared from total cellular RNA using a High Pure RNA isolation kit (Roche) following the manufacturer's instructions, was used as a template for nested PCR with the following design. In the first reaction, a primer specific for either gene of interest (for putG3PDH1, 5'-CAGAGTAACCGGAGGCAAAAT-3'; for mtG3PDH1, 5'-CAGCTTTTCAAGGTAACGGATA-3') was used together with a primer derived from the splice leader (SL) RNA gene (SL1 [5'-ACTAAC GCTATTATTAGAACAGTTCC-3']). In the second step, one of the gene-specific primers (for putG3PDH2, 5'-GCAAAATCACCCGACC-3'; for mtG3PDH2, 5'-ACGGATACCACCGTGAATGA-3') was mixed with primer SL2 (5'-TATTAGAACAGTTCTGTACTATATTG-3') (the two primers were located closer to each other than the paired primers described above were to each other).

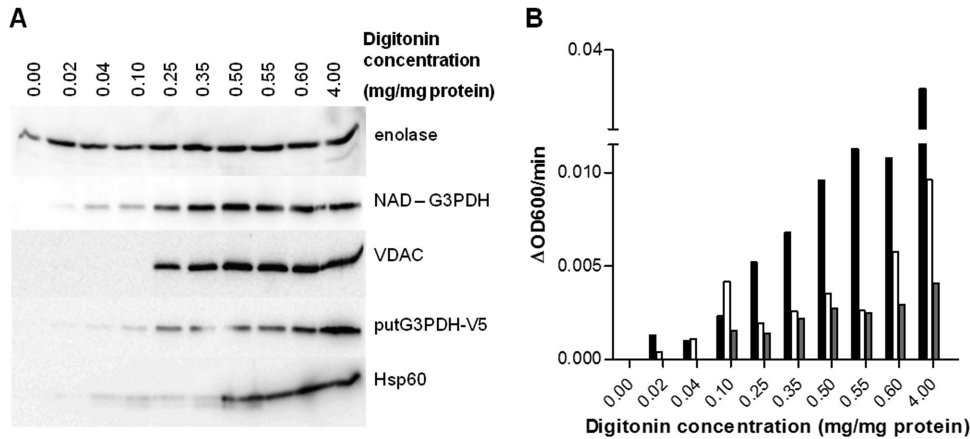


FIG 1 Analyses of supernatants obtained by digitonin fractionation. (A) Western analysis of samples treated with increasing concentrations of digitonin. Concentrations of digitonin per mg protein (ranging from 0 mg to 4 mg) are indicated. Enolase and NAD-G3PDH served as cytosolic and glycosomal markers, respectively; VDAC and Hsp60 were used as markers of the outer mitochondrial membrane and mitochondrial matrix, respectively. (B) Spectrophotometric measurements of FAD-G3PDH activity in digitonin fractions. The cell lines used were putG3PDH-V5 (black columns), noninduced (white columns), and tetracycline-induced (gray columns) mtG3PDH RNAi knockdown cells. x axis = concentration of digitonin per mg protein; y axis = FAD-G3PDH activity in ΔOD_{600} per min.

Enzymatic activities. For FAD-dependent G3PDH activity, we have modified the original protocol of Ebikeme et al. (12). This modification in our hands increased the sensitivity by approximately 3 times. A 75- μ g volume of mitochondrial lysate was added to a 1-ml cuvette containing 25 mM Tris buffer (pH 7.0), 0.075 mM 2,6-dichlorophenolindophenol, and 0.1 mM phenazine methosulfate, and the activity was measured by recording the decrease of absorbance at 600 nm triggered by the addition of 50 mM DL-glycerol-3-phosphate (G3P).

Mitochondrial *bcl* activity was measured as described previously (27).

Digitonin permeabilization. This experiment was performed following modifications described elsewhere (28). A 15-ml volume of exponential-growth culture ($\sim 1.5 \times 10^7$ cells/ml) was spun for 10 min ($1,500 \times g$ at room temperature), and the resuspended pellet was washed twice in STE buffer (250 mM sucrose, 10 mM Tris-HCl [pH 7.4], 1 mM EDTA). Next, the protein concentration was determined using the Bradford assay, and the pellets were divided into aliquots containing 150 μ g of protein each and resuspended in digitonin lysis buffer (50 mM NaCl, 50 mM imidazole/HCl [pH 7.0], 2 mM aminocaproic acid, 1 mM EDTA) supplemented with increasing concentrations of digitonin (for final concentrations, see Fig. 1) to a final volume of 150 μ l. Aliquots were incubated on ice for 5 min followed by 10 min of centrifugation ($21,400 \times g$ at 4°C). The resulting pellets and/or supernatants were either resuspended in SDS-PAGE loading buffer (62.5 mM Tris-HCl [pH 6.8], 10% glycerol, 2% SDS, 2.5% 2-mercaptoethanol, 0.0025% bromophenol blue), incubated for 30 min at 37°C, and loaded on an SDS-PAGE gel or immediately used for the determination of enzymatic activities.

Western blot analyses. Digitonin-extracted fractions were separated on 12% SDS-PAGE gels and blotted onto nitrocellulose membranes, which were probed with rabbit polyclonal antibodies (Abs) against the *T. brucei* enolase (dilution, 1:150,000), heat shock protein Hsp60 (1:1,000), glycosomal NAD-G3PDH (kindly provided by P. Michels) (1:1,000), voltage-dependent anion channel (VDAC; kindly provided by A. Schneider) (1:1,000), and mouse monoclonal Ab against the V5 tag (Sigma-Aldrich) (1:1,000). Appropriate secondary Abs (Sevapharma) (1:2,000) coupled to horseradish peroxidase were visualized using an ECL kit according to the manufacturer's protocol (Pierce). For specification of band intensities, Manual Rectangle Selection of regions of interest (ROIs) was used (Kodak Molecular Imaging Software).

Isolation of mitochondria and preparation of cell and mitochondrial lysates. Mitochondria were isolated from 5×10^8 cells by hypotonic lysis as described previously (27). Mitochondrial pellets were stored at

-80°C for spectrophotometric measurements of the G3PDH activity. To obtain cleared lysates, either isolated mitochondria or 5×10^8 cells were incubated with 2% (wt/vol) dodecylmaltoside in 0.5 M aminocaproic acid in a final volume of 50 μ l on ice for 1 h and then spun at $21,000 \times g$ for 30 min at 4°C. Supernatants were kept on ice until further use.

Phospholipid extraction and TLC analysis. A 5-ml volume of exponential culture was centrifuged and washed in STE buffer, and pelleted cells were resuspended in 1 ml of a chloroform:methanol:water mixture (10:10:3). The mixture was then transferred into a clean glass tube, and upon the addition of 100 mg glass beads (0.5 mm in diameter), the mixture was subjected to a vortex procedure 6 times (at maximum speed for 1 min with 1 min of incubation on ice). The lower layer was carefully separated, avoiding any uptake of glass beads, and kept on ice. The remaining supernatant was replaced with 500 μ l of extraction mixture, and the extraction was repeated. The lower layer was combined with the first aliquot and dried using a SpeedVac. The dried sample was extracted using a butanol:water mixture (1:1), and the upper phase was recovered and dried using a SpeedVac. The dried sample was dissolved in a chloroform:methanol mixture (2:1) and transferred onto a thin layer chromatography (TLC) plate (TLC aluminum sheets with silica gel 60; Merck).

Phospholipids were separated using a chloroform:methanol:water mixture (65:25:4). Upon reaching the front side, the plate was air-dried and submerged into a visualization solution containing 10% CuSO_4 and 8% H_3PO_4 . The TLC plate was then dried at 130°C until bands became visible.

Localization of putG3PDH in *S. cerevisiae* and *T. brucei*. Both localization procedures were performed using a FluoView 1000 (Olympus) confocal microscope, and yEGFP was detected at 488 nm. Yeast mitochondria were stained using 5 nM Mitotracker Red (Invitrogen)—growth medium for 30 min and visualized at 594 nm. Samples were mounted by the use of Vectashield mounting medium with 1.5 μ g/ml DAPI (4',6-diamidino-2-phenylindole) (Vector Laboratories), and the visualization was performed at 470 nm.

Staining and immunofluorescence analyses of the *T. brucei* PF were performed either with Mitotracker Red and a single Ab or with two different Abs. For Mitotracker Red staining, the dye was added to 3 ml of exponential culture to reach a final concentration of 1 μ M and the culture was then gently agitated for 30 min at 27°C .

For immunofluorescence, trypanosomes were washed in phosphate-buffered saline (PBS), resuspended in fresh 4% formaldehyde, and settled onto poly-L-lysine coated slides. Slides were fixed with ice-cold methanol

for 1 h, briefly rehydrated in PBS, and incubated for 2 h with the primary Ab followed by three washes in PBS. They were then incubated with fluorescein-conjugated secondary Alexa Fluor 488 (anti-rabbit) and/or Alexa Fluor green (anti-mouse) Ab (Life Technologies) (both 1:1,000). Primary antibodies were used in the following combinations: Mitotracker Red with α -V5-tagged Ab (10 μ g/ml), α -V5-tagged Ab with rabbit polyclonal Ab against glycosomal GAPDH (glyceraldehyde-3-phosphate dehydrogenase) (kindly provided by P. Michels) (1:10,000), and, finally, α -V5-tagged Ab with α -enolase Ab (1:10,000).

Images were manipulated using GNU Image Manipulation Program (GIMP) 2.6.8 software. Raw pictures were normalized using Automatic Normalization followed by Curves manipulation to decrease nonspecific background spotting.

Flow cytometry. Analysis of mitochondrial membrane potential was performed as described previously (29). Briefly, the cells were stained using 60 nM TMRE (tetramethylrhodamine, ethyl ester) (Invitrogen) directly in the medium. To assess the physiological zero potential, carbonyl cyanide 4-(trifluoromethoxy) phenylhydrazone (FCCP) was added to reach a final concentration of 10 μ M. Flow cytometry was performed using BD FACSCanto II and analyzed in FACSDiva and CyfLogic software. A total of 20,000 cells were analyzed in each run.

Respiration of digitonin-permeabilized cells. A respiration experiment was performed as described previously (29). Briefly, cells were counted, pelleted, and resuspended in manitol buffer (0.65 M manitol, 10 mM Tris, 40 mM KPi; pH 6.8) at a concentration of 10^8 cells/ml. An aqueous solution of digitonin was added to reach a final concentration of 150 μ g/ml, and the permeabilized cells were incubated on ice for 5 min and then pelleted and resuspended in the same volume of the respiration buffer supplemented with a mixture consisting of 10 mM MgSO₄, 2.5 mg/ml fatty acid-free bovine serum albumin (BSA), and 1 mM ADP. Respiration was recorded using a Clark-type electrode following 4 min of stabilization in 50 mM DL-glycerol-3-phosphate–10 mM Tris-HCl (pH 7.0) or 10 mM NADH–water.

RESULTS

Expression of FAD-G3PDHs. Expression of both genes coding for FAD-G3PDH was evaluated using the SL RNA-based strategy. cDNA prepared from total RNA was used as a template for nested PCR performed with two pairs of SL RNA-specific primers. Attachment of the SL RNA to the 5' end of the mRNA via *trans*-splicing provides evidence that the gene is transcribed into a translatable mRNA. Sequencing-confirmed ~350-bp-long amplicons provide evidence that mtG3PDH and putG3PDH are expressed in both the PF and BF cells (30).

***In silico* and *in vivo* subcellular localization of putG3PDH.** The gene database entry at www.genedb.org predicts for putG3PDH two alternative intracellular compartments: the mitochondrion, predicted by MitoCarta (17), and the endoplasmic reticulum (F. Opperdoes, personal communication). To clarify this conundrum, we amplified the whole ORF from strain 29-13 and cloned it into two different plasmids with C-terminal tags: pLew79 bearing a V5 tag for analysis of expression in *T. brucei* and pUG35 bearing yEGFP for analysis of expression in *S. cerevisiae*.

In the amplified ORF, several nonsynonymous mutations were found that are also present in the putG3PDH sequence obtained from strain 427 (available at www.tritrypdb.org). Sequence differences between the putG3PDHs from strains 427 and 927 are marked in Fig. S1 and S2 in the supplemental material. Although the overall secondary structure is conserved, the N termini (amino acids 1 to 11) of the two proteins differ as a consequence of two mutations, F10L and A17V, with strain 427 being the reference. While that strain possesses in this region a mostly helical structure (average confidence prediction, 55%), strain 927 bears a predom-

inantly coiled structure with a rather low (40%) average confidence prediction. *In silico* analysis of subcellular localization using WoLF PSORT (31) predicted mitochondrial localization of the putG3PDH gene product from the 427 strain, while its homologue from strain 927 was predicted to lack any mitochondrial import signal. Further analysis showed that the two above-mentioned N-terminal mutations are indeed responsible for the different *in silico* predictions, as a change of either of the two amino acids present in strain 427 was sufficient to again support *in silico* mitochondrial localization (see Table S1 in the supplemental material).

We have optimized the expression of putG3PDH-V5 and compared it with the expression of COX6-V5 (COX6 is a subunit of respiratory complex IV in the same vector). The COX6-V5 protein was detected with antibodies against both the V5 tag and COX6 itself (see Fig. S4 in the supplemental material). The results showed that COX6-V5 represents only a small part of the total COX6 protein; most of COX6-V5 is assembled into complex IV, and the level of expression of putG3PDH-V5 is lower than that of COX6-V5. These facts strongly support the interpretation that putG3PDH-V5 is not strongly overexpressed and that, with high probability, the V5 tag has no negative effect on the function of putG3PDH-V5 (see Fig. S4 in the supplemental material).

Using digitonin titration, the subcellular localization of putG3PDH was experimentally addressed in cells expressing the V5-tagged version of the protein, as increasing concentrations of this nonionic detergent sequentially permeabilize cell membranes on the basis of their different levels of sterol content (32). Marker Abs for different *T. brucei* cell compartments were used as controls (Fig. 1A). While the enolase was released at the lowest digitonin concentrations, the majority of glycosomal NAD-G3PDH and all mitochondrial outer membrane-specific VDAC were released at a higher concentration (0.25 mg digitonin/mg protein). Finally, mitochondrial inner membrane and matrix proteins, represented by Hsp60, were efficiently released only at a high concentration (0.5 mg digitonin/mg protein) (Fig. 1A). The putG3PDH-V5 protein was released from the pellet along with VDAC, suggesting that the studied enzyme is predominantly localized within one of the mitochondrial membranes and most likely not in another organelle (Fig. 1A). Along with digitonin extraction, we fractionated cells using silicon carbide (see Fig. S3 [E] in the supplemental material). This experiment confirmed the mitochondrial localization of putG3PDH. The pattern of putG3PDH-V5 localization correlated with the activity of mitochondrial complex III (Fig. S3 [B and C]) as well as with that of the matrix Hsp70 protein (Fig. S3 [D]).

To further address the localization of putG3PDH, 12 h after its expression was induced, the V5-tagged protein was followed by immunofluorescence. In the PF cells, its signal invariably colocalized with that of the Mitotracker Red-stained mitochondrion, strongly indicating that this organelle is the site of putG3PDH-V5 residence (Fig. 2A). Control immunofluorescence experiments were performed with Ab against glycosomal GAPDH and enolase (Fig. 2A). Moreover, this result was independently confirmed in the yeast system. Yeast cells bearing a methionine-regulated ectopic copy of the *T. brucei* putG3PDH gene fused with yEGFP at its C terminus showed in the confocal microscope a strong green signal exclusively colocalizing with Mitotracker Red (Fig. 2B). Thus, we propose the mitochondrion as the place of residence of the putG3PDH protein.

FAD-G3PDH activity in subcellular fractions. Supernatants

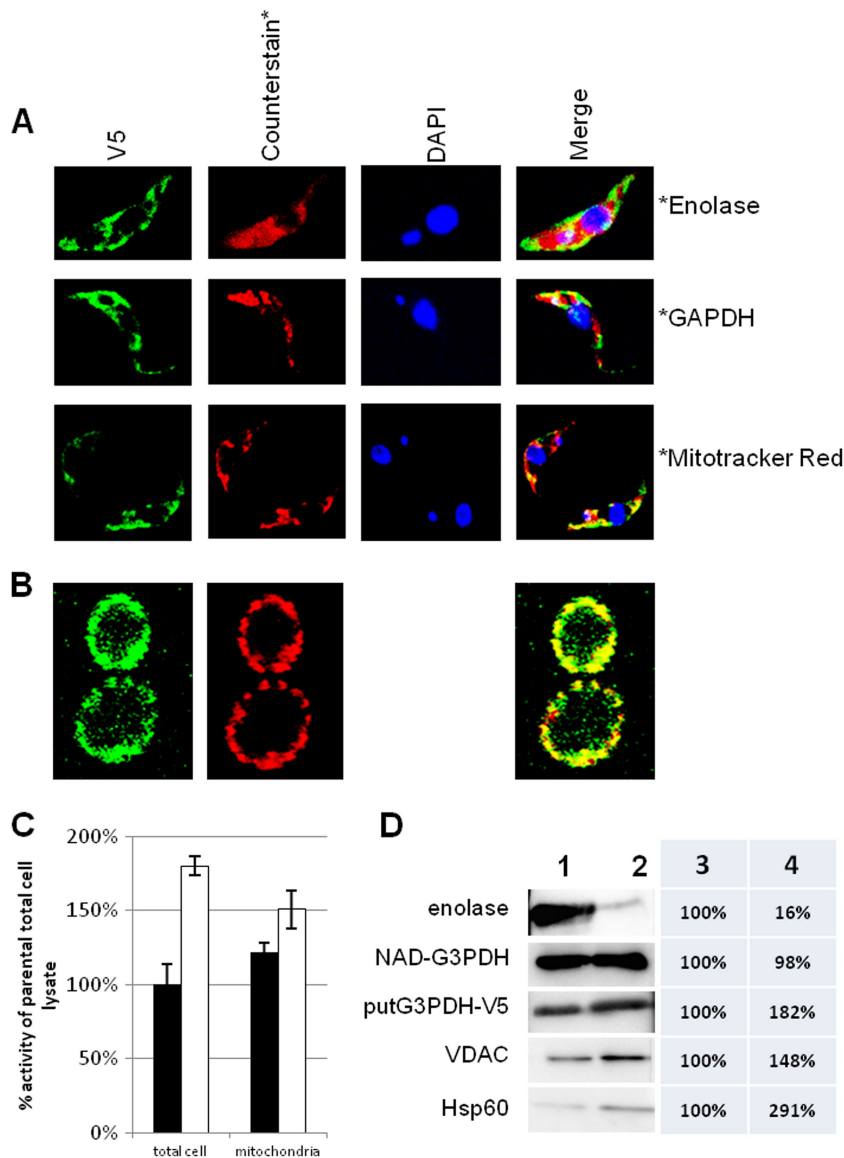


FIG 2 Localization of tagged putG3PDH and its effect on G3PDH activity. Confocal microscopy shows the distribution of the overexpressed putG3PDH-V5 after 12 h of induction in *T. brucei* PF. (A) Antibodies against enolase and GAPDH and Mitotracker Red dye were used to visualize the cytosolic, glycosomal, and mitochondrial compartments, respectively. The Merge column shows the overlap of V5 signal with the mitochondrion. (B) Confocal microscopy analysis of *S. cerevisiae* expressing TbputG3PDH-yEGFP. The cells were stained using Mitotracker Red (red signal), and the green signal corresponds to yEGFP fluorescence. (C) Comparison of the levels of FAD-G3PDH activity upon expression of putG3PDH-V5 in the parental 29-13 cell line and in cells overexpressing putG3PDH for 12 h. Averages and standard deviations of the results are shown for total cell and mitochondrial lysates of putG3PDH-V5 cells (white columns) and strain 29-13 cells (black columns). y axis = FAD-G3PDH activity expressed as a percentage of the parental strain level. (D) Comparison of the relative levels of proteins in whole cells and in hypotonically isolated mitochondria. Lysates of cells (lanes 1 and 3) and hypotonically isolated mitochondria (lanes 2 and 4) were resolved by electrophoresis in 12% SDS gel, and Western analysis was performed with antibodies against V5 epitope and cytosolic (enolase), glycosomal (NAD-G3PDH), mitochondrial outer membrane (VDAC), and mitochondrial matrix (Hsp60) proteins (lanes 1 and 2). The intensity of the signal in the cell fraction was defined as 100% for each tested protein, and the relative intensity of the appropriate signal in the mitochondrial fraction was calculated (lanes 3 and 4).

obtained after digitonin treatment were used for a spectrophotometric assay of the FAD-G3PDH activity. In the absence of digitonin, the pellet contained intact cells and no activity was measured in the supernatant. Increasing concentrations of the detergent caused increases in the release of the FAD-G3PDH activity from the pellet, derived sequentially from the cytosol, the single-membrane organelles, and, finally, the mitochondrion.

The FAD-G3PDH activity was determined in the putG3PDH-V5

cell line with the aim to check whether the tagged protein still retains its activity. A major increase of activity was recorded in the fraction treated with 0.25 mg digitonin/mg protein (Fig. 1B), corresponding to the lower putG3PDH-V5 signal in the Western blot analysis (Fig. 1A). The activity increased linearly and reached a plateau at 0.55 mg digitonin/mg protein. That remarkable jump represents the concentration of 4 mg digitonin/mg protein that released all proteins from the cells. It led to a 3-fold increase in

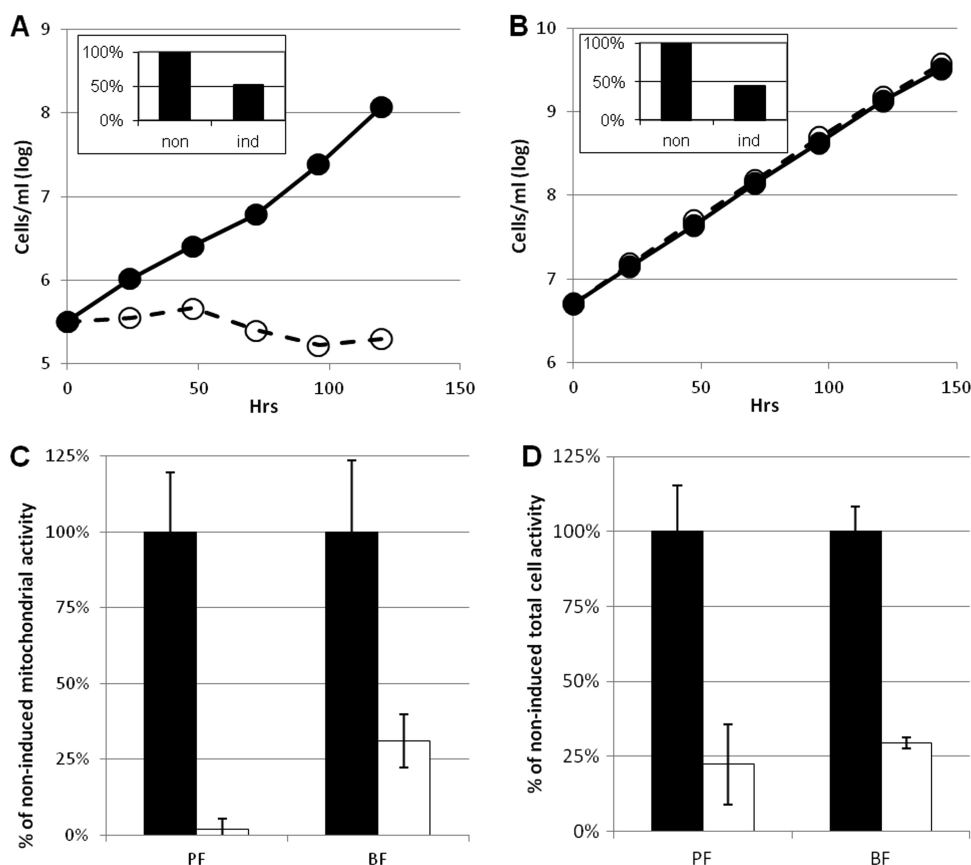


FIG 3 Phenotypic analysis of mtG3PDH knockdowns. (A and B) Growth phenotype of BF (A) and PF (B) *T. brucei* tested against mtG3PDH. Full and dashed lines correspond to the noninduced (non) and RNAi-induced (ind) cells, respectively. x axis = hours after induction; y axis = cell concentration/ml (log scale). The insets show the level of depletion of the mtG3PDH mRNA 4 days after RNAi induction, as assessed by qPCR using 18S rRNA as a reference. (C and D) Comparison of levels of RNAi-mediated ablation of the mtG3PDH activity in mitochondrial lysates (C) or total lysates (D) from PF and BF cells. Percentages of average activity \pm standard deviations (SD) in noninduced (black columns) and RNAi-induced (white columns) cells are shown. Activity in the noninduced cells represents 100%.

FAD-G3PDH activity in the putG3PDH-V5 cells ($\sim 0.03 \Delta\text{OD}/\text{min}$ for 4 mg of digitonin compared to $\sim 0.01 \Delta\text{OD}/\text{min}$ for 0.6 mg of digitonin). In all fractions in which putG3PDH-V5 was released, the measured FAD-G3PDH activity was remarkably higher than that seen with the noninduced mtG3PDH cells (see below), strongly associating the FAD-G3PDH activity with putG3PDH-V5.

We have also measured the FAD-G3PDH activity on whole-cell lysates and hypotonically isolated mitochondria obtained from the putG3PDH-V5 cell line (12 h after induction of expression) and the parental strain. The putG3PDH-V5 activity was confirmed by the massive increase of activity observed in total lysates of the tagged cell line compared to the lysates of the wild-type cells ($+80\% \pm 7\%$). However, a small yet statistically significant (Mann-Whitney U-test; see Table S2 in the supplemental material) increase in the activity occurred in the putG3PDH-V5-containing mitochondria ($+24\% \pm 11\%$) (Fig. 2C), suggesting that putG3PDH is weakly associated with this organelle. To assess the purity of the hypotonically isolated mitochondria, we probed total cell and mitochondrial lysates with the same antibodies as were used for screening the digitonin fractions (Fig. 2D). Although the hypotonically isolated mitochondria are contaminated with glycosomal proteins, the mitochondrial fraction is en-

riched for proteins from both the mitochondrial matrix and the outer mitochondrial membrane, as shown by signals of Hsp60 and VDAC, respectively. This fraction was also enriched for the G3PDH-V5 construct.

We then tried to test the activity of putG3PDH-V5 directly by isolating the pure protein by immunoprecipitation using a protein G Sepharose matrix (see Fig. S5 in the supplemental material). Lysate from the cells expressing putG3PDH-V5 had G3PDH activity that was two times higher than the activity seen with the parental strain (data not shown). However, there was no measurable activity in the sample with putG3PDH-V5 bound to the protein G Sepharose with antibodies against the V5 tag, probably a consequence of tight interaction between putG3PDH-V5 and the affinity Sepharose. We were not able to release it from the matrix using natural conditions, and even boiling released the protein only partially (see Fig. S5 in the supplemental material).

Depletion of mtG3PDH. To establish the relative contributions of mtG3PDH and putG3PDH to the total cellular FAD-G3PDH activity, we prepared cell lines of both life stages with mtG3PDH inducibly ablatable by RNAi and collected total RNA from cells 4 days after RNAi induction. Quantitative RT-PCR confirmed downregulation of the mtG3PDH transcript by 50% to 60% (Fig. 3A and B [insets]).

Growth of the noninduced and RNAi-induced cells was monitored, and the cells were daily diluted back to the initial concentration. Confirming the data by Ebikeme et al. (12), the PF cells ablated for mtG3PDH showed no growth retardation, and the enzyme is therefore nonessential for this life cycle stage (Fig. 3B). In contrast, the BF cells grew slower from the very beginning of RNAi induction. On day 1 and 3, the induced cells reached only 34% and 4%, respectively, of the concentration of their noninduced counterparts. On the fourth day, the cultures were virtually dead (Fig. 3A).

The FAD-G3PDH activity was measured in either total cells or mitochondrial lysates 3 days after RNAi induction and compared with the same activity in the noninduced cells (Fig. 3C and D; see also Table S3 in the supplemental material). Downregulation of mtG3PDH expression resulted in 70% (PF) and 80% (BF) decreases of the FAD-G3PDH activity in total cell extracts. Ebikeme et al. (12) did not find any residual FAD-dependent G3PDH activity in whole PF cell lysates after ablation of mtG3PDH. It is quite possible that the residual activity remained under the detection limit of their measurement due to the lower sensitivity of the assay used (in our hands, the measured activity was 3 times higher than the activity level published in reference 12). The remaining 20% to 30% of activity probably corresponds to the contribution of putG3PDH. To test this hypothesis, the activity was recorded in the noninduced and RNAi-induced cells permeabilized by digitonin (Fig. 1B; white and gray columns). In the noninduced cells, an initial release of the FAD-G3PDH activity appeared with 0.1 mg digitonin/mg protein, followed by a second release at 0.6 mg digitonin/mg protein (Fig. 1B). The RNAi-induced cells lacked the second wave of FAD-G3PDH activity, which was clearly attributable to mtG3PDH located in the mitochondrial inner membrane.

mtG3PDH in mitochondrial metabolism and physiology. In a previous study of an alternative NADH:ubiquinone oxidoreductase (NDH2), we observed elevated and reduced respiration on G3P and NADH, respectively, upon RNAi-mediated depletion of NDH2, probably due to the upregulated expression of mtG3PDH (29). To see whether the downregulation of mtG3PDH has the opposite effect, a respiratory experiment with digitonin-permeabilized PF cells was performed 6 days after RNAi induction, with G3P and NADH as the respiratory substrates (Fig. 4A). As expected, a massive decrease of respiration on G3P occurred; however, NADH did not show any significant change (Mann-Whitney U-test P value = 0.2). Other mitochondrial functions, namely, the activities of respiratory complexes II, III, and IV, did not change (data not shown).

Since cells RNAi depleted for NDH2 show decreased mitochondrial membrane potential and yet increased *in vitro* mtG3PDH activity (29), we decided to perform the same measurements in the PF cells ablated for mtG3PDH. The cells were induced for 3 days, stained with TMRE, and analyzed by flow cytometry, and the uncoupler FCCP was used as a control. A representative output of a typical experiment (Fig. 4B and C) illustrates that in the RNAi-induced cells only a minor change of distribution leads to the shift in median fluorescence, corresponding to an approximately 20% decrease of mitochondrial membrane potential (Fig. 4D).

In *T. brucei*, synthesis of phospholipids starts with the conversion of glycolysis-generated G3P (33) to phosphatidic acid in a two-step reaction (EC 2.3.1.15) ($G3P + \text{acyl-coenzyme A [CoA]} \rightarrow$

$1\text{-acyl-G3P}; 1\text{-acyl-G3P} + \text{acyl-CoA} \rightarrow \text{phosphatidic acid [1,2-diacyl-glycerol-3-phosphate]}$). In the following steps, phosphatidylcholine (PC), phosphatidylethanolamine (PE), phosphatidylserine (PS), phosphatidylinositol (PI), and cardiolipin are produced, with the last-named compound requiring additional condensation of G3P. To evaluate whether ablation of mtG3PDH has an impact on the phospholipid metabolism, we analyzed the extracted phospholipids on TLC plates. Neither PC nor PE and PI showed any change in the RNAi knockdowns or the putG3PDH-V5 cells (data not shown). While other phospholipids were repeatedly identified, cardiolipin was undetectable.

DISCUSSION

The glycerol-3-phosphate:dihydroxyacetone phosphate (G3P:DHAP) shuttle represents a key link between glycolysis and mitochondrial metabolism. While the presence of several different forms of NAD-G3PDH is relatively common in eukaryotes (15, 16), two isoforms of FAD-G3PDH are, as far as we know, unique to trypanosomatids. To date, TAO and other components of the respiratory chain have been subjected to numerous investigations (8, 12, 14, 27, 29, 34–41), while only two studies dealt with the function of mtG3PDH (12, 14), and the role of putG3PDH remains totally unknown.

Both genes are expressed throughout the life cycle of *T. brucei*, which is in accordance with an earlier report (14) as well as transcriptomic analyses (30, 42, 43), with both of them showing more than 2-fold upregulation of putG3PDH mRNA in the PF cells. Indeed, in a comparative SILAC study, the putG3PDH protein was detected 5 times more often in PF than in BF (44), and yet two other studies using the same protein-labeling method failed to detect putG3PDH at all (45, 46) (see Table S4 in the supplemental material). Although this discrepancy might reflect different proteomics approaches, one cannot exclude the possibility that it has been influenced by the different cultivation media and strains used (44–46).

In the absence of Ab against any of the FAD-G3PDH isoforms, we have used the tagging strategy to independently address localization of putG3PDH in the PF flagellates. Western blot analysis of fractions obtained by the digitonin permeabilization and immunolocalization data of the C-tagged putG3PDH allowed establishing intracellular localization of the studied proteins. First, along with its genuine mitochondrial import signal, *T. brucei* putG3PDH has been expressed as a yEGFP fusion in yeast. The same approach was successfully used by Guerra et al. (14) for localizing mtG3PDH in the mitochondrion. Although the robustness of the expression varied depending on the carbon source used for cultivation (data not shown), the protein invariably colocalized with Mitotracker Red, confirming its mitochondrial localization. Second, using immunofluorescence, the V5-tagged putG3PDH was localized to the single-branched mitochondrion of *T. brucei*, which is in agreement with the *in silico*-predicted localization for the strain 427-derived isoform; the localization of the strain 427-derived isoform remains an open issue, as *in silico* analysis did not reveal any targeting signal. However, this observation is likely to reflect the data sets used for application training. Combined with all our obtained data, we propose the mitochondrial outer membrane to be likely the membrane housing putG3PDH. The idea that it is an appurtenance to this compartment is further supported by the detection of putG3PDH in the *T. brucei* outer membrane mitoproteome (47). However, contrary to

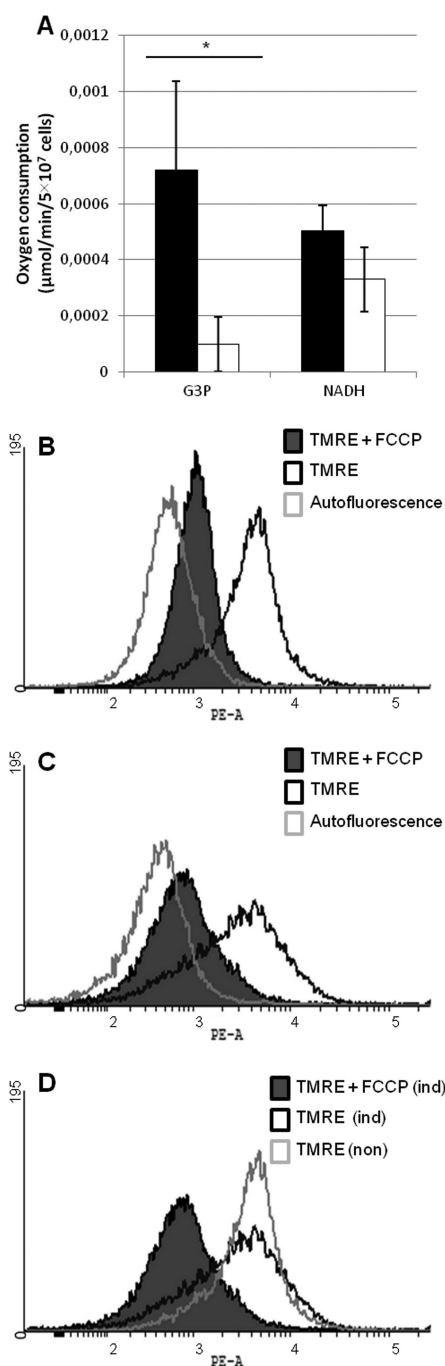


FIG 4 Effect of mtG3PDH knockdown on mitochondrial physiology. (A) Respiration of permeabilized PF downregulated for mtG3PDH with NADH and G3P as the substrates. Respiration was measured following permeabilization by digitonin in the noninduced cells (black columns) and RNAi-induced cells (white columns). The *x* axis depicts alternative substrates (G3P and NADH). The *y* axis shows oxygen consumption ($\mu\text{mol}/\text{min}/5 \times 10^7$ cells). An asterisk (*) denotes a significant difference (Mann-Whitney U-test; $\alpha = 0.05$). Data are representative of the output of flow cytometer analysis of the mitochondrial membrane potential of the PF mtG3PDH mutant. (B and C) Non-induced (B) and induced (C) RNAi cell lines. Cells were analyzed without staining to evaluate their autofluorescence (gray line). TMRE-stained cells (black line) and TMRE-stained cells with FCCP (black line, gray filling) were compared. (D) Overlay of TMRE-stained noninduced (gray line) and induced (black line) cells compared with the induced TMRE-stained cells in the presence of FCCP (black line, gray filling). *x* axes in panels B to D represent relative fluorescence values; *y* axes represent a histogram of cell counts.

our conclusions, putG3PDH was also detected in the crude preparation of the mitochondrial inner membrane, although this identification was based on only a single unique peptide compared to the 21 unique peptides corresponding to mtG3PDH (47), suggesting that the inner mitochondrial membrane preparation was contaminated with material from the outer membrane.

Digitonin-extracted cellular fractions were also instrumental in the measurement of the FAD-G3PDH activity. While its relative activity in the parental cells was higher in the organellar fraction than in the total cell lysate, the situation was the opposite in the cell line overexpressing putG3PDH-V5. We believe that the relatively low increase of the organellar FAD-G3PDH activity is in this case likely due to the nature of isolation, as the hypotonically isolated mitochondria probably lost part of an outer membrane. This assumption fits with the observation that an RNAi knockdown of mtG3PDH leads to almost complete depletion of the G3PDH activity in the mitochondrial fraction, while there is still up to 20% of the FAD-G3PDH activity in total cell lysates. Our data may also explain the early observations of Allemann and Schneider, who described findings indicating that hypotonically isolated mitochondria were unable to synthesize ATP upon the addition of G3P (10). Furthermore, they observed that the overall FAD-G3PDH activity dropped by half in the hypotonically treated and yet isotonicly isolated organelles (10). All available data are therefore compatible with localization of putG3PDH in the outer mitochondrial membrane (Fig. 5), despite the absence of direct evidence to prove this localization.

Next, we wanted to establish the relative contributions of the two FAD-G3PDHs to the cellular metabolism of *T. brucei*. In contrast to PF, the BF cells do not contain a succinate-producing branch in their glycosomes (9) and hence exclusively regenerate the reduced cofactors required for glycolysis via the G3P:DHAP shuttle using mtG3PDH (13, 14). The importance of mtG3PDH for the BF cells is further reflected by its upregulation compared to PF in this life stage at both the RNA level (42, 43) and the protein level (44–46). The essentiality of mtG3PDH for BF is therefore not surprising, while depletion of the same protein in PF, reflected in the absence of its respective enzymatic activity, did not result in an altered growth phenotype, regardless of whether regular or low-glucose SDM-79 medium was used (data not shown). Although mtG3PDH is also expressed in PF, its contribution to the mitochondrial electron transport chain seems to be negligible or non-existent, which is also reflected by the lack of any significant changes in the mitochondrial membrane potential. The data further confirm a previous observation of the utilization of mtG3PDH upon loss of the glycosomal succinate-producing branch (12).

Increasing FAD-G3PDH activity in the tag-bearing cells confirmed the ability of putG3PDH to perform FAD-dependent conversion of G3P to DHAP. However, measurement of the FAD-G3PDH activity in the digitonin fractions of noninduced and RNAi-induced mtG3PDH mutants excluded the possibility of upregulation of putG3PDH as a means for the cells to cope with the drop in the mtG3PDH activity. The best way to get an insight into the physiological function of putG3PDH would be depletion of the protein in PF. Unfortunately, repeated attempts to generate viable RNAi cell lines targeting this protein have so far failed.

Due to its localization outside the inner mitochondrial membrane and its FAD-G3PDH activity, putG3PDH function may be related to the maintenance of the cellular redox balance but with a

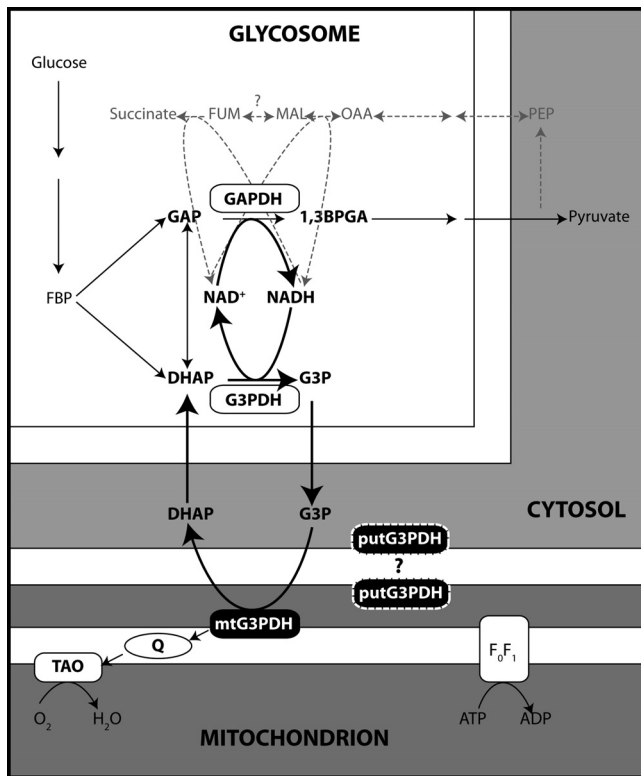


FIG 5 Schematic representation of energy metabolism of glycosome and its connection with mitochondrion. Data represent subcellular localization of G3PDHs in *T. brucei* and their involvement in biochemical pathways. Thin black arrows represent glucose degradation common for PF and BF. Bold black arrows represent a G3P:dihydroxyacetone phosphate shuttle and its integration into the glycosomal redox balance in BF. Gray dotted arrows represent a redox balancing pathway specific for PF. G3PDH is a glycosomal NAD-dependent isoform; mtG3PDH is the mitochondrial FAD-dependent isoform that constitutes the shuttle. putG3PDH represents the second FAD-dependent isoform with an unknown role in cellular metabolism (see the text). Boxes represent enzymes: GAPDH, glycosomal glyceraldehyde-3-phosphate dehydrogenase; F_0F_1 , mitochondrial complex V/ATPase; TAO, trypanosomal alternative oxidase. Q in an oval represents coenzyme Q/ubiquinol. Abbreviations represent metabolic intermediates: 1,3BPGA, 1,3-bisphosphoglycerate; DHAP, dihydroxyacetone phosphate; FBP, fructose biphosphate; FUM, fumarate; GAP, glyceraldehyde-3-phosphate; G3P, glycerol-3-phosphate; MAL, malate; OAA, oxaloacetate; PEP, phosphoenolpyruvate. ?, a place of reaction is not certain, i.e., glycosome versus cytosol for fumarase and intermembrane space-facing versus cytosol-facing for putG3PDH.

role different from that of mtG3PDH. Because of its possible outer mitochondrial membrane localization, which remains to be clearly demonstrated, we propose that putG3PDH is particularly involved in the glycosomal redox balance (Fig. 5). The PF cells have developed several pathways to reoxidize NADH produced in the glycosomes, such as the organellar succinate-producing branch and the DHAP:G3P shuttle involving mtG3PDH (14). The above-described upregulation of putG3PDH in PF (42, 44) indicates that this enzyme may to some extent replace mtG3PDH in this life stage. Theoretically, putG3PDH could indeed replace mtG3PDH or compete with it for the same G3P substrate, since the two enzymes share the FAD-G3PDH activity. However, while mtG3PDH uses ubiquinol as an electron acceptor to keep its FAD cofactor oxidized, putG3PDH does not seem to have direct access to the quinone pool. Consequently, FAD bound to putG3PDH

might shuffle its electrons to an electron transfer flavoprotein, should any be available. Indeed, several electron-transfer flavoproteins (ETF) have been detected in the *T. brucei* genome. A recent study on the mitochondrial outer membrane proteome (47) detected three and two ETFs in the inner and outer membrane clusters, respectively. Such an ample presence of ETFs in the membranes makes it tempting to speculate that putG3PDH could be coupled by one of them to the ETF:ubiquinone oxidoreductase localized in the inner mitochondrial membrane. However, at this stage we cannot exclude the alternative possibility that putG3PDH regenerates cytosolic DHAP and ultimately transfers electrons to another terminal acceptor (mtG3PDH uses molecular oxygen) yet to be identified or performs the reverse reaction, utilizing DHAP to produce G3P, which would be even more intriguing.

ACKNOWLEDGMENTS

We thank Karolína Šubrtová (University of South Bohemia) for help with some experiments, Jozef Nosek and Michaela Jakúbková (Comenius University) for consultations and technical support of experiments with the yeast system, and Paul A. M. Michels (Universidad de los Andes/University of Edinburgh) and André Schneider (University of Bern) for antibodies.

This work was supported by the Czech Grant Agency (P305/11/2179 and 206/09/H026), the Czech Ministry of Education (AMVIS LH12104), and the Praemium Academiae award to J.L., by the Scientific Grant Agency of the Slovak Ministry of Education and the Academy of Sciences (1/0393/09 and 1/0664/13), and by National Scholarship Programme of the Slovak Republic for the Support of Mobility to Z.V. and ITMS 26240120027, supported by the Research & Development Operational Programme funded by the ERDF. J.L. is a Fellow of the Canadian Institute for Advanced Research. We acknowledge the use of research infrastructure that has received funding from the European Union Seventh Framework Programme (FP7/2007-2013) under grant agreement no. 316304.

REFERENCES

- Kennedy PGE. 2012. An alternative form of melarsoprol in sleeping sickness. *Trends Parasitol.* 28:307–310.
- Bringaud F, Rivière L, Coustou V. 2006. Energy metabolism of trypanosomatids: adaptation to available carbon sources. *Mol. Biochem. Parasitol.* 149:1–9.
- van Weelden SWH, Fast B, Vogt A, Van der Meer P, Saas J, Van Hellemond JJ, Tielens AGM, Boshart M. 2003. Procytic *Trypanosoma brucei* do not use Krebs cycle activity for energy generation. *J. Biol. Chem.* 278:12854–12863.
- van Hellemond JJ, Opperdoes FR, Tielens AGM. 2005. The extraordinary mitochondrion and unusual citric acid cycle in *Trypanosoma brucei*. *Biochem. Soc. Trans.* 33:967–971.
- Opperdoes FR. 1987. Compartmentation of carbohydrate metabolism in trypanosomes. *Annu. Rev. Microbiol.* 41:127–151.
- Opperdoes FR, Borst P, Bakker S, Leene W. 1977. Localization of glycerol-3-phosphate oxidase in the mitochondrion and particulate NAD⁺-linked glycerol-3-phosphate dehydrogenase in the microbodies of the bloodstream form of *Trypanosoma brucei*. *Eur. J. Biochem.* 76:29–39.
- Fang J, Beattie DS. 2002. Rotenone-insensitive NADH dehydrogenase is a potential source of superoxide in procyclic *Trypanosoma brucei* mitochondria. *Mol. Biochem. Parasitol.* 123:135–142.
- Surve S, Heestand M, Panicucci B, Schnauffer A, Parsons M. 2012. Enigmatic presence of mitochondrial complex I in *Trypanosoma brucei* bloodstream forms. *Eukaryot. Cell* 11:183–193.
- Michels PAM, Bringaud F, Herman M, Hannaert V. 2006. Metabolic functions of glycosomes in trypanosomatids. *Biochim. Biophys. Acta* 1763:1463–1477.
- Allemann N, Schneider A. 2000. ATP production in isolated mitochondria of procyclic *Trypanosoma brucei*. *Mol. Biochem. Parasitol.* 111:87–94.
- Opperdoes FR, Borst P. 1977. Localization of nine glycolytic enzymes in a microbody-like organelle in *Trypanosoma brucei*: the glycosome. *FEBS Lett.* 80:360–364.

12. Ebikeme C, Hubert J, Biran M, Gouspillou G, Morand P, Plazolles N, Guegan F, Diolez P, Franconi J-M, Portais J-C, Bringaud F. 2010. Ablation of succinate production from glucose metabolism in the procyclic trypanosomes induces metabolic switches to the glycerol 3-phosphate/dihydroxyacetone phosphate shuttle and to proline metabolism. *J. Biol. Chem.* 285:32312–32324.
13. Clarkson AB, Bienen EJ, Pollakis G, Grady RW. 1989. Respiration of bloodstream forms of the parasite *Trypanosoma brucei brucei* is dependent on a plant-like alternative oxidase. *J. Biol. Chem.* 264:17770–17776.
14. Guerra DG, Decottignies A, Bakker BM, Michels PAM. 2006. The mitochondrial FAD-dependent glycerol-3-phosphate dehydrogenase of Trypanosomatidae and the glycosomal redox balance of insect stages of *Trypanosoma brucei* and *Leishmania* spp. *Mol. Biochem. Parasitol.* 149:155–169.
15. Gee RW, Byerrum RU, Gerber DW, Tolbert NE. 1988. Differential inhibition and activation of two leaf dihydroxyacetone phosphate reductases: role of fructose 2,6-bisphosphate. *Plant Physiol.* 87:379–383.
16. Wei Y, Periappuram C, Datla R, Selvaraj G, Zou J. 2001. Molecular and biochemical characterizations of a plastidic glycerol-3-phosphate dehydrogenase from *Arabidopsis*. *Plant Physiol. Biochem.* 39:841–848. doi:10.1016/S0981-9428(01)01308-0.
17. Pagliarini DJ, Calvo SE, Chang B, Sheth SA, Vafai SB, Ong S-E, Walford GA, Sugiana C, Boneh A, Chen WK, Hill DE, Vidal M, Evans JG, Thorburn DR, Carr SA, Mootha VK. 2008. A mitochondrial protein compendium elucidates complex I disease biology. *Cell* 134:112–123.
18. Panigrahi AK, Ogata Y, Zíková A, Anupama A, Dalley RA, Acestor N, Myler PJ, Stuart KD. 2009. A comprehensive analysis of *Trypanosoma brucei* mitochondrial proteome. *Proteomics* 9:434–450.
19. Wickstead B, Ersfeld K, Gull K. 2002. Targeting of a tetracycline-inducible expression system to the transcriptionally silent minichromosomes of *Trypanosoma brucei*. *Mol. Biochem. Parasitol.* 125:211–216.
20. Vondrušková E, van den Burg J, Zíková A, Ernst NL, Stuart K, Benne R, Lukeš J. 2005. RNA interference analyses suggest a transcript-specific regulatory role for mitochondrial RNA-binding proteins MRP1 and MRP2 in RNA editing and other RNA processing in *Trypanosoma brucei*. *J. Biol. Chem.* 280:2429–2438.
21. Wirtz E, Leal S, Ochatt C, Cross GA. 1999. A tightly regulated inducible expression system for conditional gene knock-outs and dominant-negative genetics in *Trypanosoma brucei*. *Mol. Biochem. Parasitol.* 99:89–101.
22. Flaspohler JA, Jensen BC, Saveria T, Kifer CT, Parsons M. 2010. A novel protein kinase localized to lipid droplets is required for droplet biogenesis in trypanosomes. *Eukaryot. Cell* 9:1702–1710.
23. Cormack BP, Bertram G, Egerton M, Gow NAR, Falkow S, Brown AJP. 1997. Yeast-enhanced green fluorescent protein (yEGFP): a reporter of gene expression in *Candida albicans*. *Microbiology* 143(Pt 2):303–311.
24. Gietz RD, Schiestl RH, Willems AR, Woods RA. 1995. Studies on the transformation of intact yeast cells by the LiAc/SS-DNA/PEG procedure. *Yeast* 11:355–360.
25. Carnes J, Trotter JR, Ernst NL, Steinberg A, Stuart K. 2005. An essential RNase III insertion editing endonuclease in *Trypanosoma brucei*. *Proc. Natl. Acad. Sci. U. S. A.* 102:16614–16619.
26. Pfaffl MW. 2001. A new mathematical model for relative quantification in real-time RT-PCR. *Nucleic Acids Res.* 29:e45. doi:10.1093/nar/29.9.e45.
27. Horváth A, Horáková E, Dunajčíková P, Verner Z, Pravidová E, Šlapetová I, Cuninková L, Lukeš J. 2005. Downregulation of the nuclear-encoded subunits of the complexes III and IV disrupts their respective complexes but not complex I in procyclic *Trypanosoma brucei*. *Mol. Microbiol.* 58:116–130.
28. Rivière L, Moreau P, Allmann S, Hahn M, Biran M, Plazolles N, Franconi J-M, Boshart M, Bringaud F. 2009. Acetate produced in the mitochondrion is the essential precursor for lipid biosynthesis in procyclic trypanosomes. *Proc. Natl. Acad. Sci. U. S. A.* 106:12694–12699.
29. Verner Z, Škodová I, Poláková S, Ďurišová-Benkovičová V, Horváth A, Lukeš J. 2013. Alternative NADH dehydrogenase (NDH2): intermembrane-space-facing counterpart of mitochondrial complex I in the procyclic *Trypanosoma brucei*. *Parasitology* 140:328–337.
30. Kabani S, Fenn K, Ross A, Ivens A, Smith TK, Ghazal P, Matthews K. 2009. Genome-wide expression profiling of in vivo-derived bloodstream parasite stages and dynamic analysis of mRNA alterations during synchronous differentiation in *Trypanosoma brucei*. *BMC Genomics* 10:427. doi:10.1186/1471-2164-10-427.
31. Horton P, Park K-J, Obayashi T, Fujita N, Harada H, Adams-Collier CJ, Nakai K. 2007. WoLF PSORT: protein localization predictor. *Nucleic Acids Res.* 35:W585–W587.
32. Wiemer EA, Hannaert V, Van den Ijssel PR, Van Roy J, Opperdoes FR, Michels PAM. 1995. Molecular analysis of glyceroldehyde-3-phosphate dehydrogenase in *Trypanoplasma borelli*: an evolutionary scenario of subcellular compartmentation in kinetoplastida. *J. Mol. Evol.* 40:443–454.
33. Creek DJ, Chokkathukalam A, Jankevics A, Burgess KEV, Breitling R, Barrett MP. 2012. Stable isotope-assisted metabolomics for network-wide metabolic pathway elucidation. *Anal. Chem.* 84:8442–8447.
34. Fang J, Beattie DS. 2003. Alternative oxidase present in procyclic *Trypanosoma brucei* may act to lower the mitochondrial production of superoxide. *Arch. Biochem. Biophys.* 414:294–302.
35. Chaudhuri M, Ott RD, Hill GC. 2006. Trypanosome alternative oxidase: from molecule to function. *Trends Parasitol.* 22:484–491.
36. Nakamura K, Fujioka S, Fukumoto S, Inoue N, Sakamoto K, Hirata H, Kido Y, Yabu Y, Suzuki T, Watanabe Y, Saimoto H, Akiyama H, Kita K. 2010. Trypanosome alternative oxidase, a potential therapeutic target for sleeping sickness, is conserved among *Trypanosoma brucei* subspecies. *Parasitol. Int.* 59:560–564.
37. Kido Y, Sakamoto K, Nakamura K, Harada M, Suzuki T, Yabu Y, Saimoto H, Yamakura F, Ohmori D, Moore A, Harada S, Kita K. 2010. Purification and kinetic characterization of recombinant alternative oxidase from *Trypanosoma brucei brucei*. *Biochim. Biophys. Acta* 1797:443–450.
38. Gnipová A, Panicucci B, Paris Z, Verner Z, Horváth A, Lukeš J, Zíková A. 2012. Disparate phenotypic effects from the knockdown of various *Trypanosoma brucei* cytochrome c oxidase subunits. *Mol. Biochem. Parasitol.* 184:90–98.
39. Verner Z, Čermáková P, Škodová I, Kriegová E, Horváth A, Lukeš J. 2011. Complex I (NADH:ubiquinone oxidoreductase) is active in but non-essential for procyclic *Trypanosoma brucei*. *Mol. Biochem. Parasitol.* 175:196–200.
40. Beattie DS, Obungu VH, Kiara JK. 1994. Oxidation of NADH by a rotenone and antimycin-sensitive pathway in the mitochondrion of procyclic *Trypanosoma brucei brucei*. *Mol. Biochem. Parasitol.* 64:87–94.
41. Fang J, Beattie DS. 2003. Identification of a gene encoding a 54 kDa alternative NADH dehydrogenase in *Trypanosoma brucei*. *Mol. Biochem. Parasitol.* 127:73–77.
42. Jensen BC, Sivam D, Kifer CT, Myler PJ, Parsons M. 2009. Widespread variation in transcript abundance within and across developmental stages of *Trypanosoma brucei*. *BMC Genomics* 10:482. doi:10.1186/1471-2164-10-482.
43. Nilsson D, Gunasekera K, Mani J, Osteras M, Farinelli L, Baerlocher L, Roditi I, Ochsenreiter T. 2010. Spliced leader trapping reveals widespread alternative splicing patterns in the highly dynamic transcriptome of *Trypanosoma brucei*. *PLoS Pathog.* 6:e1001037. doi:10.1371/journal.ppat.1001037.
44. Urbaniak MD, Guther MLS, Ferguson MAJ. 2012. Comparative SILAC proteomic analysis of *Trypanosoma brucei* bloodstream and procyclic life-cycle stages. *PLoS One* 7:e36619. doi:10.1371/journal.pone.0036619.
45. Butter F, Bucierius F, Michel M, Čičová Z, Mann M, Janzen CJ. 2013. Comparative proteomics of two life cycle stages of stable isotope-labeled *Trypanosoma brucei* reveals novel components of the parasite's host adaptation machinery. *Mol. Cell. Proteomics* 12:172–179.
46. Gunasekera K, Wüthrich D, Braga-Lagache S, Heller M, Ochsenreiter T. 2012. Proteome remodelling during development from blood to insect-form *Trypanosoma brucei* quantified by SILAC and mass spectrometry. *BMC Genomics* 13:556. doi:10.1186/1471-2164-13-556.
47. Niemann M, Wiese S, Mani J, Chanfon A, Jackson C, Meisinger C, Warscheid B, Schneider A. 2013. Mitochondrial outer membrane proteome of *Trypanosoma brucei* reveals novel factors required to maintain mitochondrial morphology. *Mol. Cell. Proteomics* 12:515–528.